Supporting Information

Assembly of trimeric polyoxovanadate aggregates based on $[MnV_{13}O_{38}]^{7-}$ building blocks and lanthanide cations

Ding Liu,[a] Ying Lu,*[a] Yang-Guang Li,[a] Hua-Qiao Tan,[b] Wei-Lin Chen,[a] Zhi-Ming Zhang and En-Bo Wang*[a]

[a]*Key Laboratory of Polyoxometalate Science of Ministry of Education, Faculty of Chemistry, Northeast Normal University, Changchun, Jilin 130024, People's Republic of China*

[b]*State Key Laboratory of Luminescence and Applications, Changchun Institute of Optics, Fine Mechanics and Physics, Chinese Academy of Sciences, 3888 East Nanhu Road, Changchun 130033, People's Republic of China.*

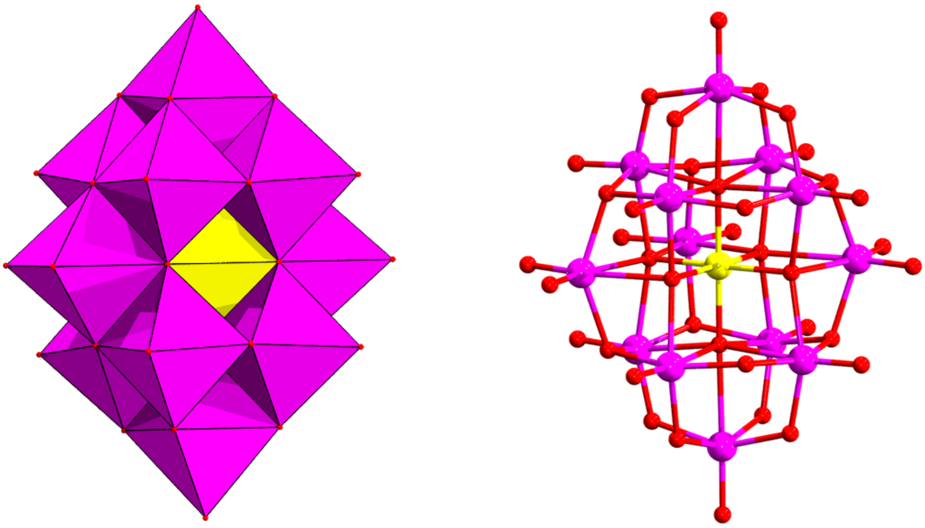

Fig. S1 Polyhedral and ball-and-stick representation of the structures of cluster $[MnV_{13}O_{38}]^{7-}$. Pink, yellow, and red represent V, Mn, and O atoms, respectively. The $[MnV_{13}O_{38}]^{7-}$ polyoxoanion consists of thirteen edge-shared VO_6 octahedra surrounding a central Mn atom in an octahedral cavity.

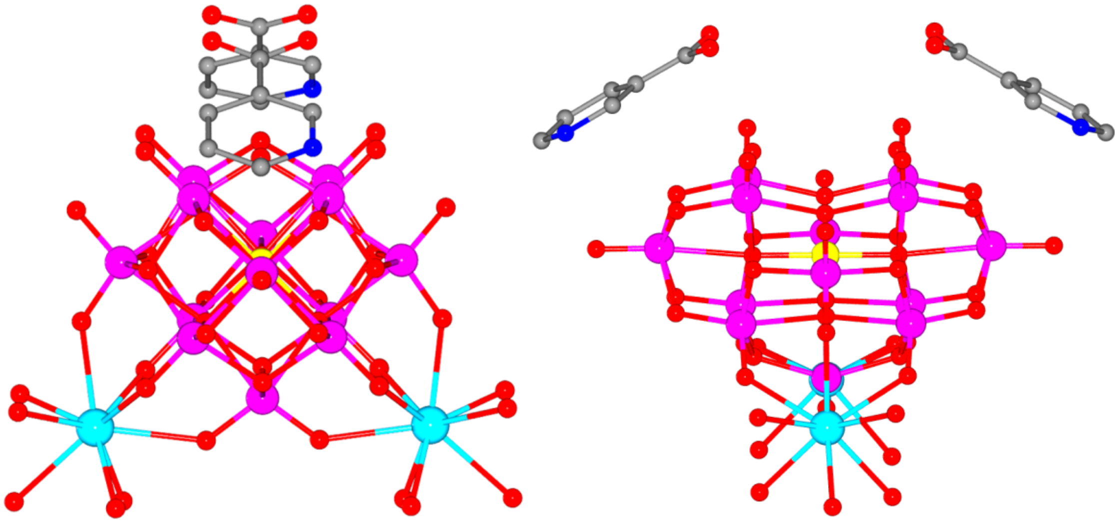

Fig. S2 Polyhedral and ball-and-stick representation of polyoxoanion $[MnV_{13}O_{38}]^{7-}$ acting as a bidentate ligand coordinating to two La^{3+} ions in compound **1**, and a pair of pyridine-3-carboxylic acid molecules interaction with the $[MnV_{13}O_{38}]^{7-}$ through hydrogen bonding on the other side.

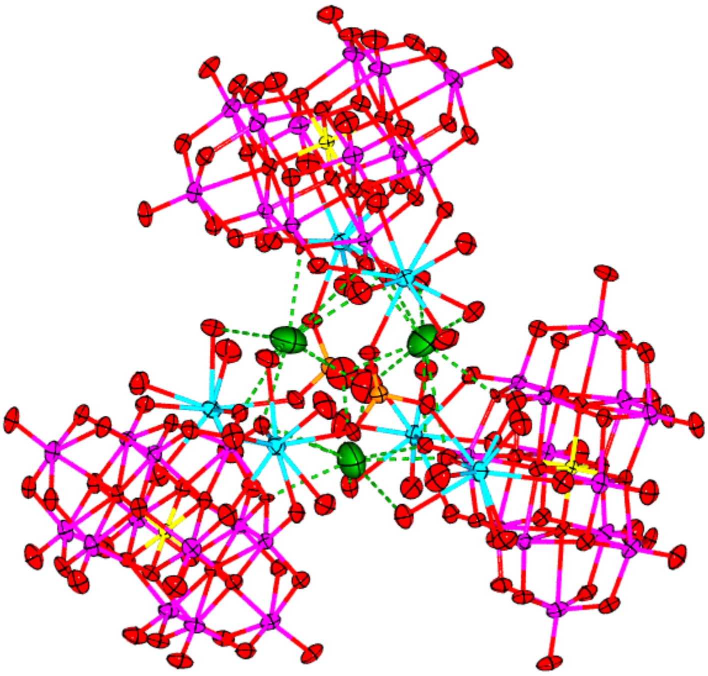

Fig. S3 ORTEP diagram of the basic structural unit in compound **1** with ellipsoids at 50 % probability displacement. The organic molecules and water molecules are omitted for clarity.

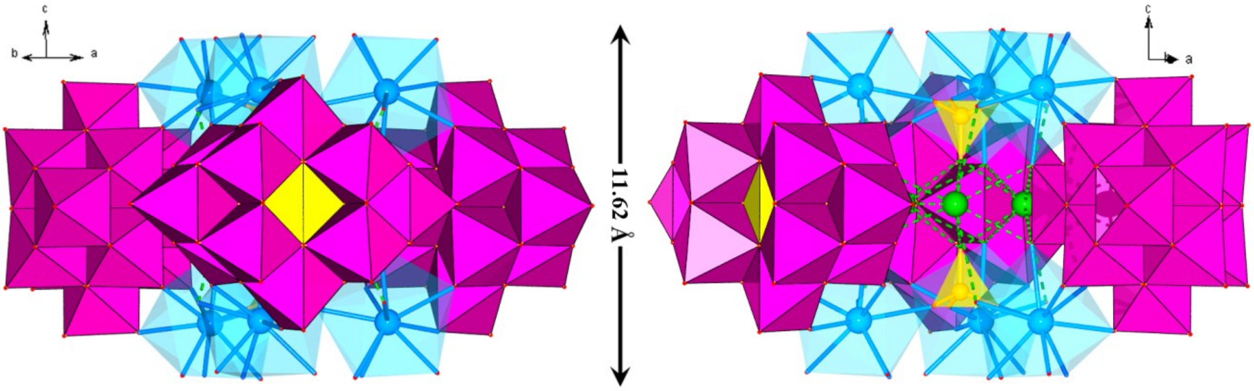

Fig. S4 View of the thickness of polyhedral and ball-and-stick representation of triple-$\{MnV_{13}\}$ polyoxoanion.

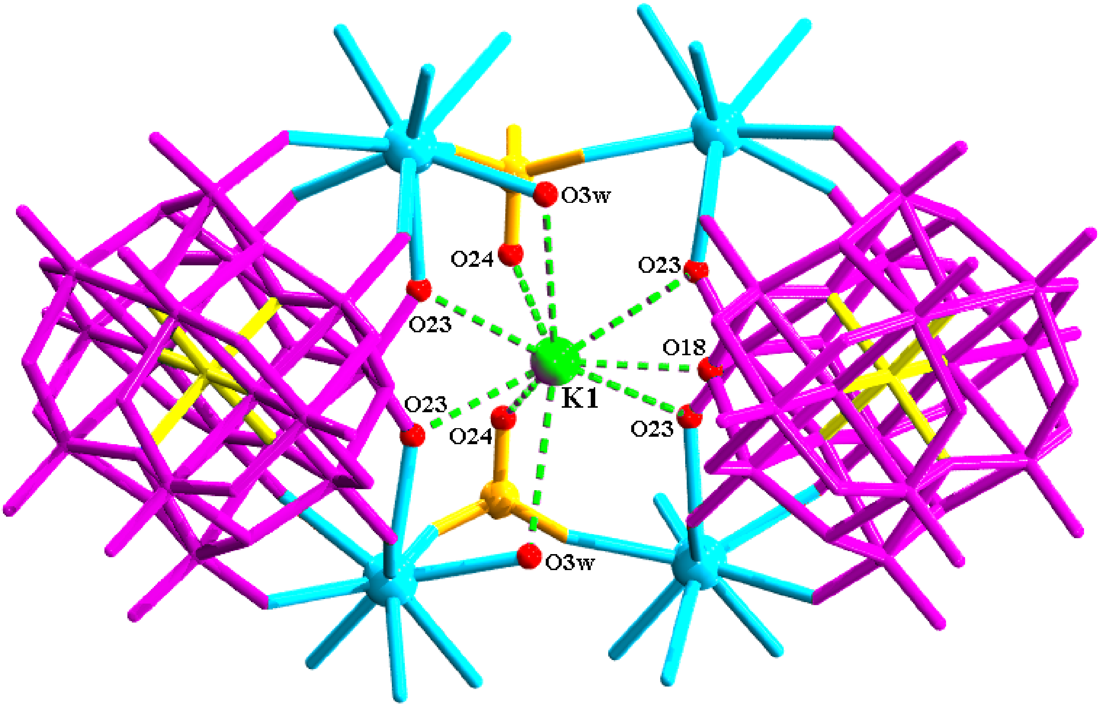

Fig. S5 Ball-and-stick representation of the coordination mode of the K^+ cation sealed in polyoxoanion **1**.

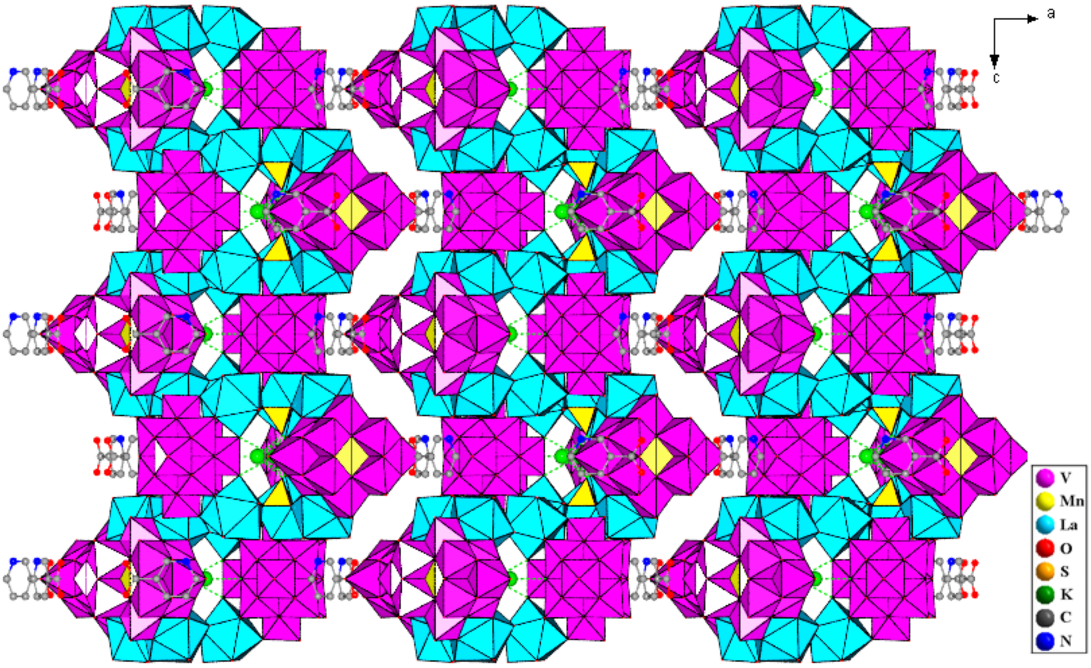

Fig. S6 Polyhedral and ball-and-stick representation of the packing arrangements of **1** along *b* axis.

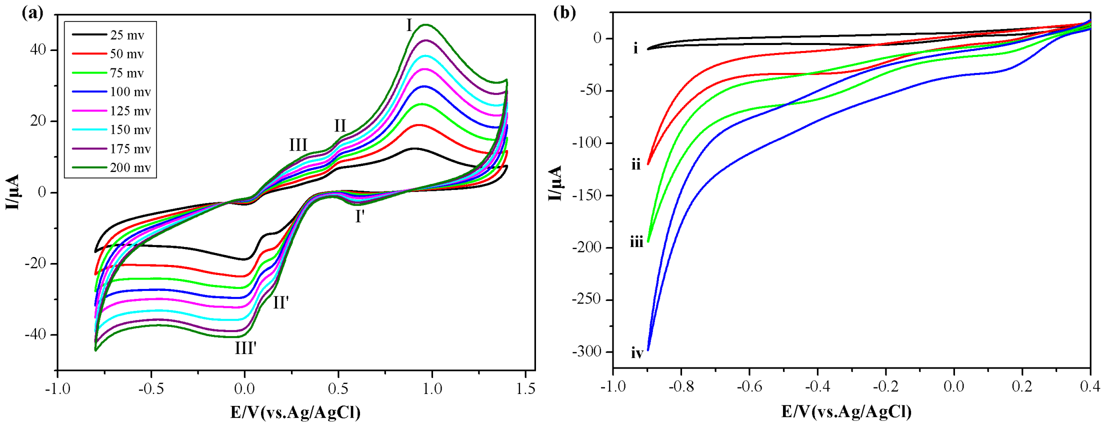

Fig. S7 (a) The cyclic voltammograms of 2 × 10^{-4} M **2** in the pH 4 (0.4 M CH_3COONa + CH_3COOH) buffer solution at the scan rates (from inner to outer: 25, 50, 75, 100, 125, 150, 175, 200 mV s^{-1}); (b) Electrocatalysis of the reduction of NO_2^- in the presence of 2 × 10^{-4} M **2** at the scan rate of 150 mV s^{-1} with NO_2^-concentrations of (i) 0.0, (ii) 1.0, (iii) 2.0, and (iv) 4.0 mM. The working electrode was glassy carbon, and the reference electrode was Ag/AgCl.

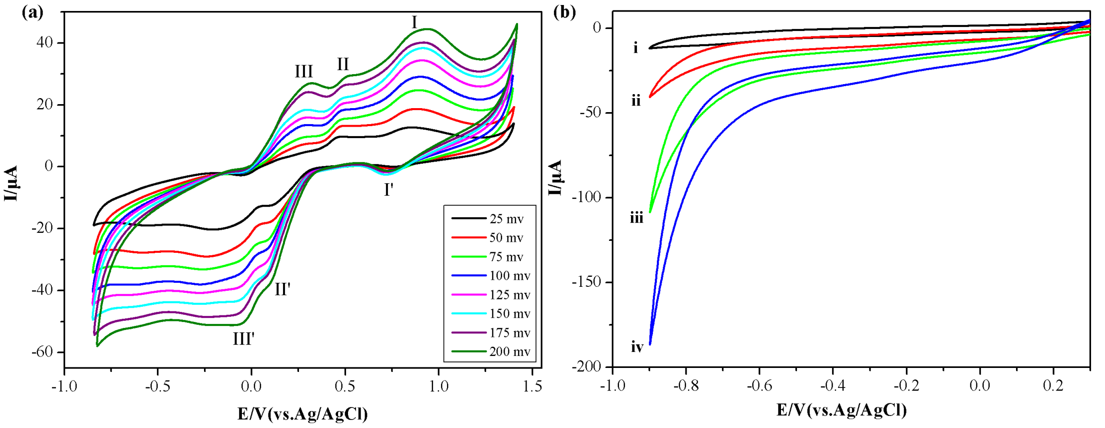

Fig. S8 (a) The cyclic voltammograms of 2 × 10^{-4} M **3** in the pH 4 (0.4 M CH_3COONa + CH_3COOH) buffer solution at the scan rates (from inner to outer: 25, 50, 75, 100, 125, 150, 175, 200 mV s^{-1}); (b) Electrocatalysis of the reduction of NO_2^- in the presence of 2 × 10^{-4} M **3** at the scan rate of 150 mV s^{-1} with NO_2^-concentrations of (i) 0.0, (ii) 1.0, (iii) 2.0, and (iv) 4.0 mM. The working electrode was glassy carbon, and the reference electrode was Ag/AgCl.

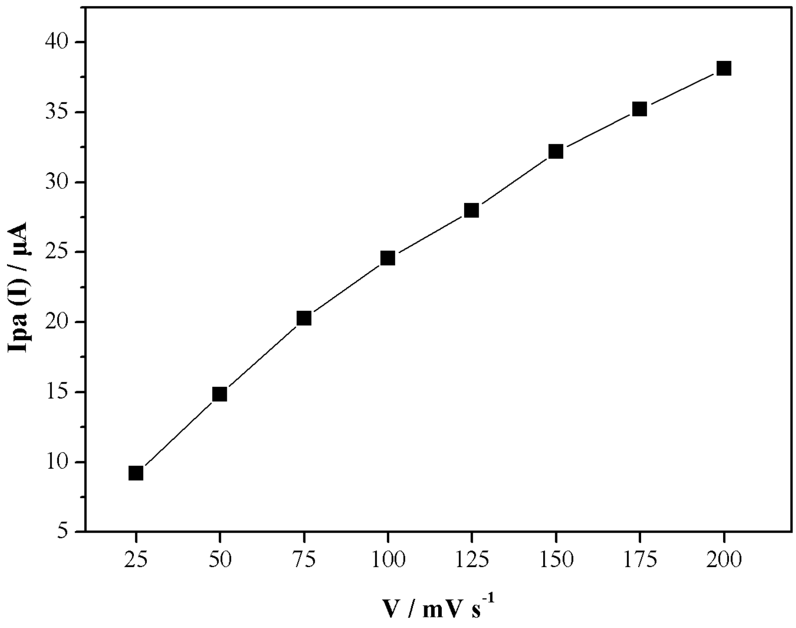

Fig. S9 The dependence of anodic peak I currents of **1** on scan rates.

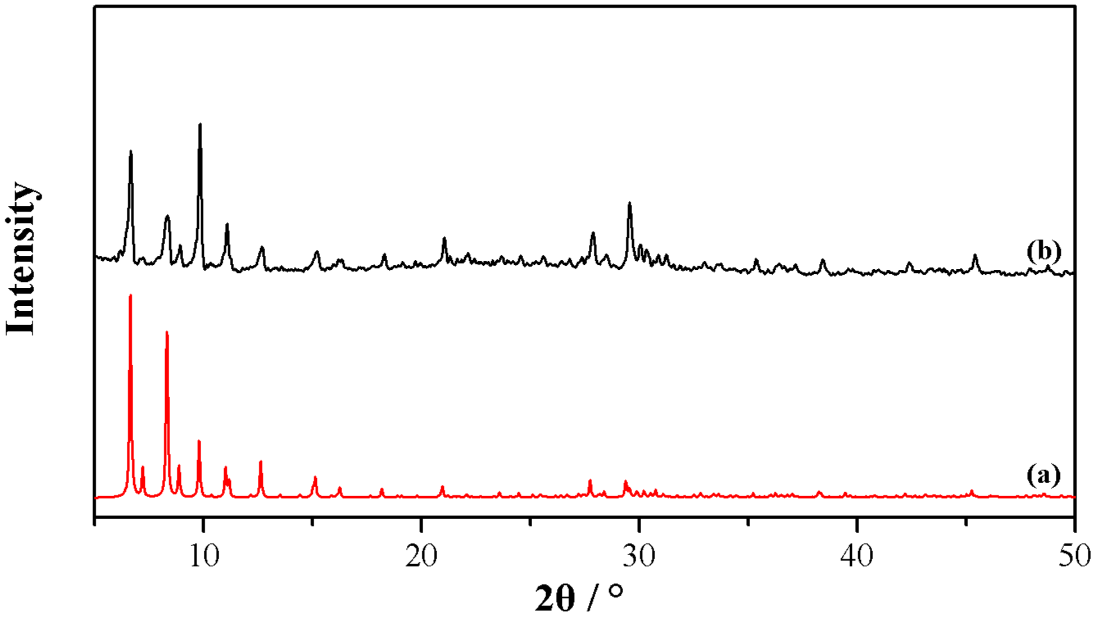

Fig. S10 XPRD patterns of compound **2**: (a) calculated, (b) as-synthesized.

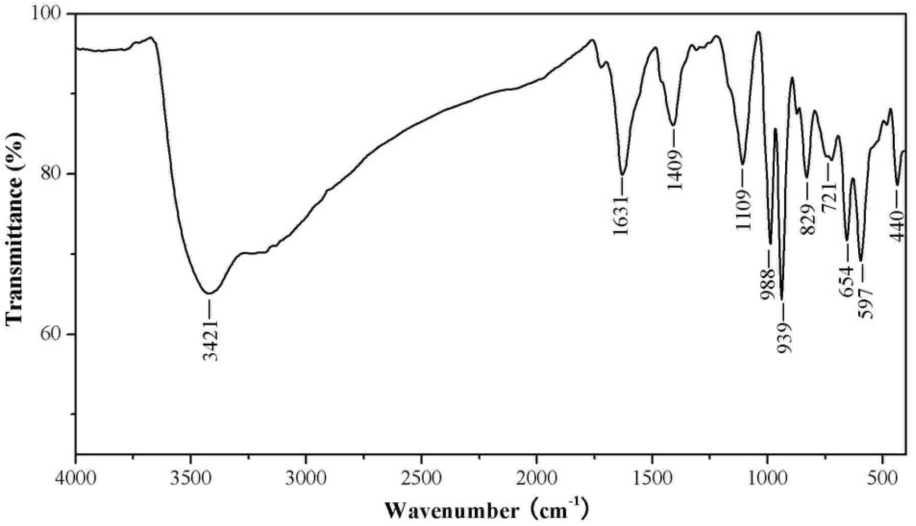

Fig. S11 IR spectrum of compound **1**.

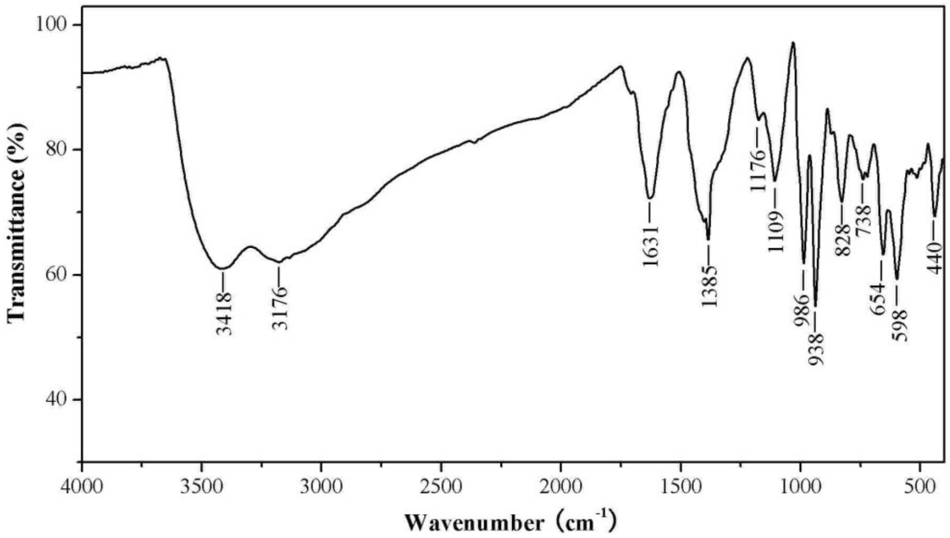

Fig. S12 IR spectrum of compound **2**.

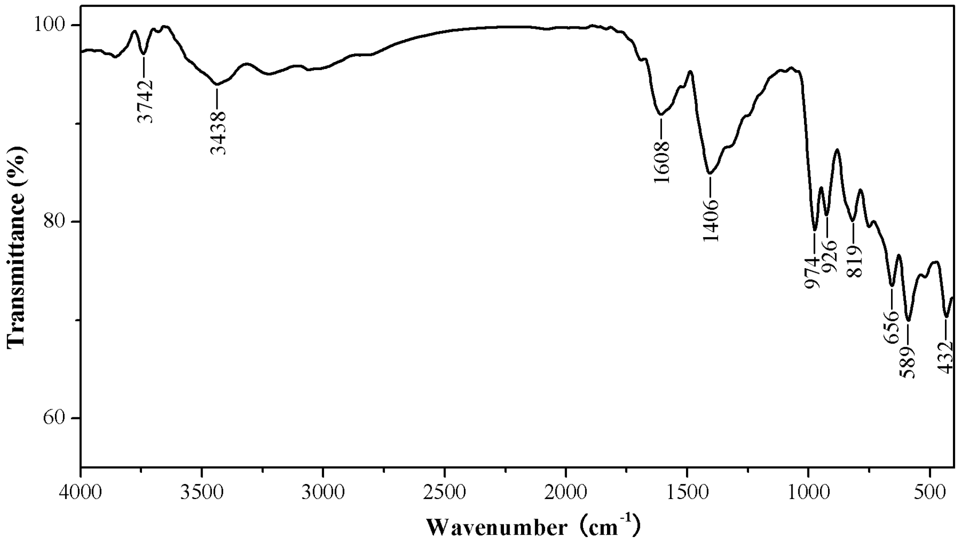

Fig. S13 IR spectrum of compound **3**.

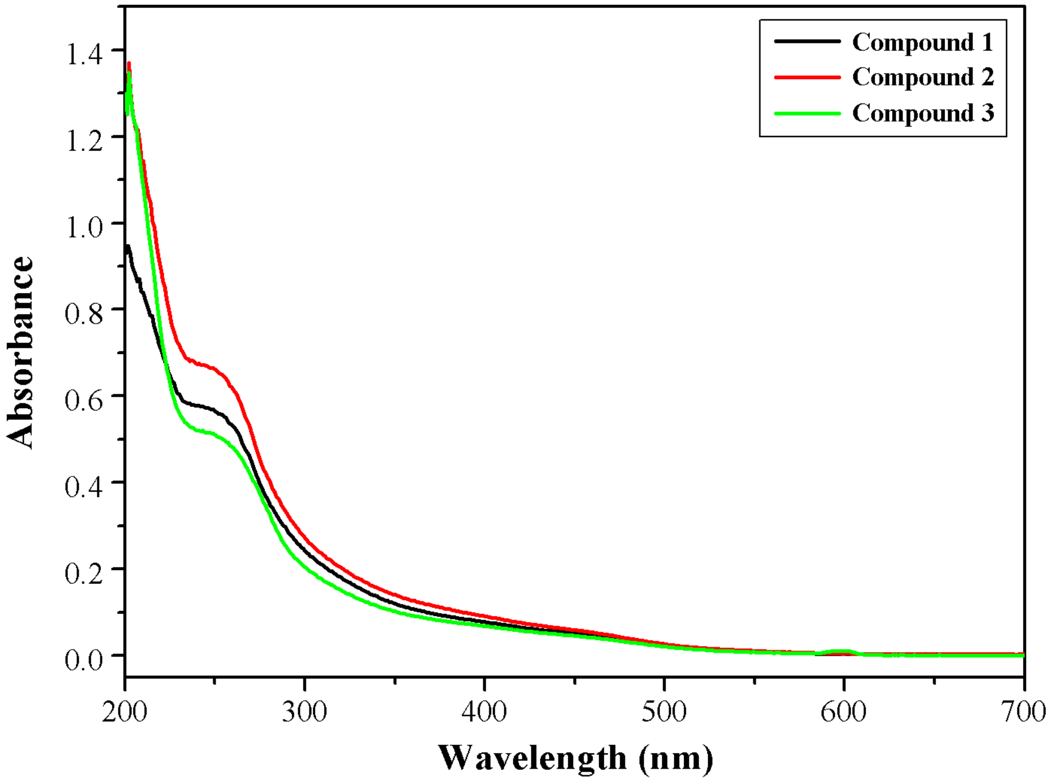

Fig. S14 The UV spectrum of **1-3** in the solution.

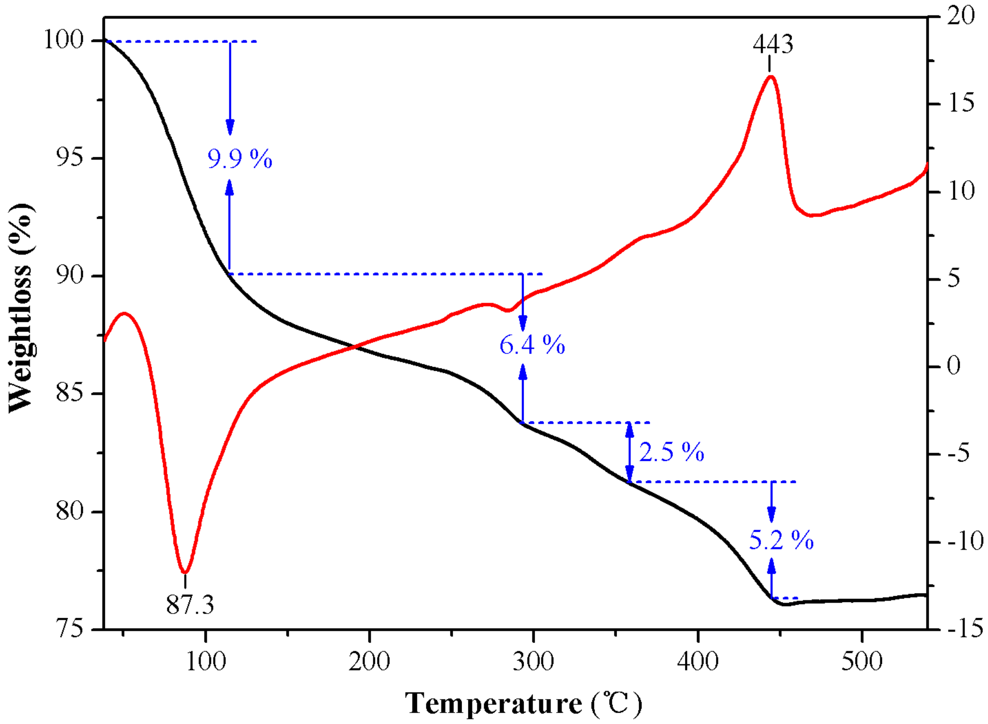

Fig. S15 The TG curve of compound **1** exhibits four continuous weight loss stages in the temperature ranges 38-445 °C. The first weight loss is 9.9 % in the temperature range 38-114 °C, corresponding to the release of lattice water molecules in the framework (calcd. 9.1 %). Then, the weight loss step of 6.4 % occurred in the temperature range of 114-294 °C, mainly corresponding to the loss of the coordinated water molecules (calcd. 6.6 %). The following weight loss of 2.5 % in the temperature range of 294-356 °C is attributed to the loss of sulfate ions (calcd. 2.9 %). The last weight loss of 5.2 % in the temperature range of 356-445 °C could be related to the loss of pyridine-3-carboxylic acid molecules and gradual elimination of carbon deposition resulting from the complex decomposition under a N_2 atmosphere (calcd. 5.7 %). The whole weight loss is 24.3 %, agreement with the theoretical weight loss value (calcd. 24 %). In the DTA curve of **1**, the endothermic broad peak around 87.3 °C corresponds to the release of lattice and coordinated water molecules; The exothermic peaks at 443 °C is attributed to the decomposition of the polyoxoanion.

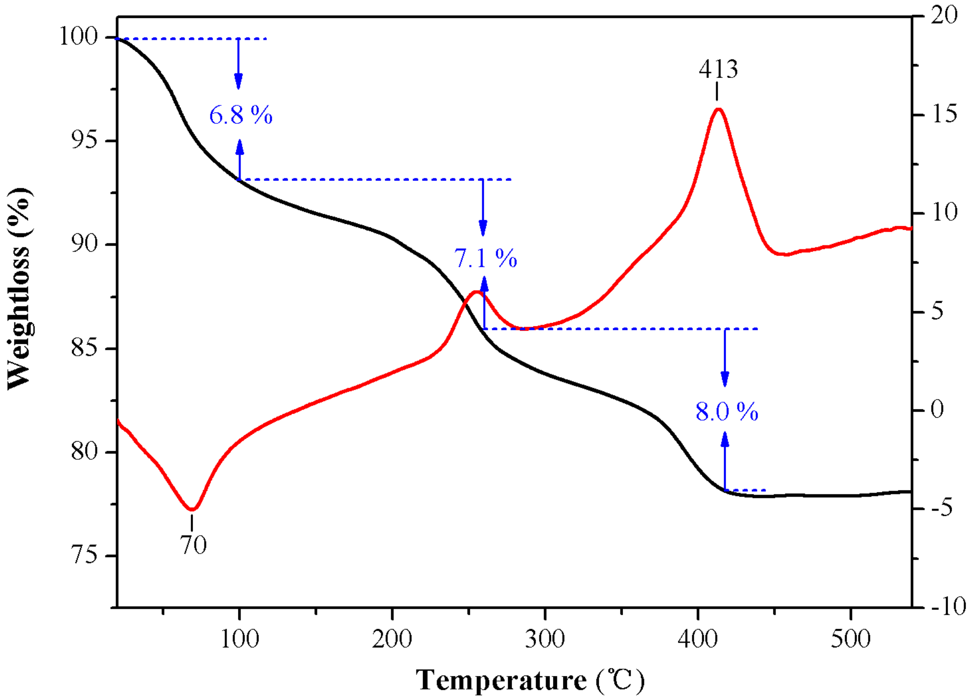

Fig. S16 The TG curve of compound **2** exhibits three continuous weight loss stages in the temperature ranges 18-421 °C. The first weight loss is 6.8 % in the temperature range 18-100 °C, corresponding to the release of lattice water molecules in the framework (calcd. 6.0 %). Then, the weight loss step of 7.1 % occurred in the temperature range of 100-259 °C, mainly corresponding to the loss of the coordinated water molecules (calcd. 6.9 %). The last two weight loss steps of 8.0 % in the temperature range of 259-418 °C could be related to the decomposition of sulfate ions and pyridine-3-carboxylic acid molecules (calcd. 8.9 %). The whole weight loss is 21.9 %, agreement with the theoretical weight loss value (calcd. 21.8 %). In the DTA curve of **2**, the endothermic broad peak around 70 °C corresponds to the release of lattice and coordinated water molecules; The exothermic peaks at 413 °C is attributed to the decomposition of the polyoxoanion.

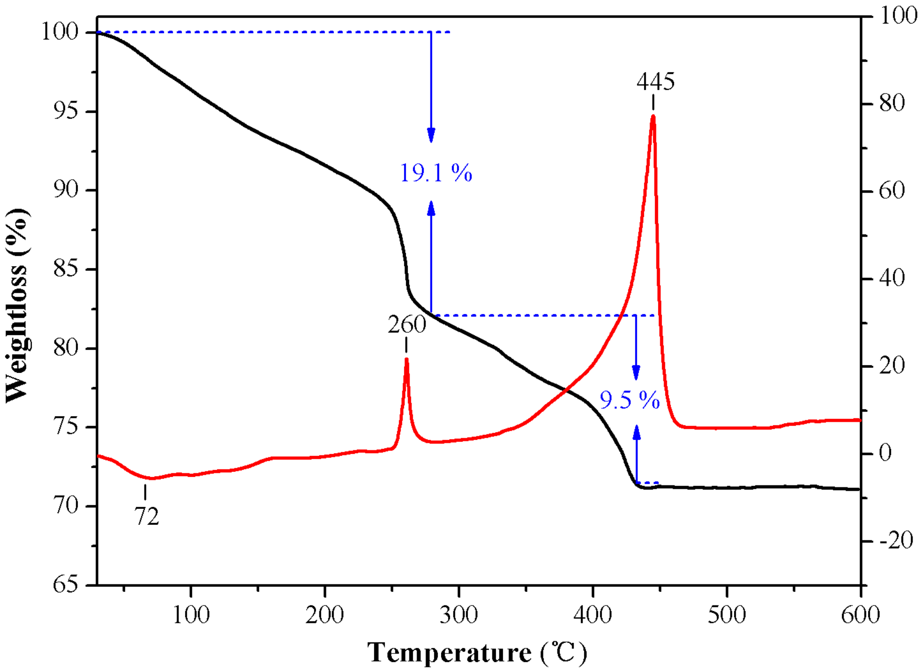

Fig. S17 The TG curve of compound **3** exhibits two continuous weight loss stages in the temperature ranges 30-434 °C. The first weight loss is 19.1 % in the temperature range 30-279 °C, corresponding to the release of lattice and coordinated water molecules in the framework (calcd. 19.6 %). The second weight loss step of 9.5 % in the temperature range of 279-434 °C could be related to the decomposition of sulfate ions and pyridine-3-carboxylic acid molecules (calcd. 8.8 %). The whole weight loss is 28.6 %, agreement with the theoretical weight loss value (calcd. 28.4 %). In the DTA curve of **3**, the endothermic broad peak around 72 °C corresponds to the release of lattice and coordinated water molecules; The exothermic peaks at 413 °C is attributed to the decomposition of the polyoxoanion.